Cancer Nanotechnology

RESEARCH

Open Access

Functional targeted therapy for glioma based on platelet membrane-coated nanogels

Qin Li[1,2†], Jinglan Shen[1,4†], Lingling Wu[3†], Siyun Lei[1], Yimin Yang[1], Weide Xu[1], Ke Hao[1,4], Yi Zhang[1,4], Fei Kong[1], Wei Yang[5], Yaling Wang[1,4], Lina Peng[1,4], Kaiqiang Li[1,4*] and Zhen Wang[1,4*]

†Qin Li, Jinglan Shen and Lingling Wu have contributed equally to this work

*Correspondence: likaiqiang@hmc.edu.cn; wangzhen@hmc.edu.cn

[1] Center for Laboratory Medicine, Allergy Center, Department of Transfusion Medicine, Zhejiang Provincial People's Hospital People's Hospital, Affiliated People's Hospital, Hangzhou Medical College, Hangzhou 310014, China
[2] Department of Clinical Laboratory, Mianyang Central Hospital, School of Medicine, University of Electronic Science and Technology of China, Mianyang 621000, People's Republic of China
[3] Women's Hospital, School Of Medicine, Zhejiang University, Hang Zhou 310014, People's Republic of China
[4] Key Laboratory of Biomarkers and In Vitro Diagnosis Translation of Zhejiang Province, Hangzhou 310063, Zhejiang, China
[5] Department of Biophysics, and Department of Neurosurgery of the First Affiliated Hospital, Zhejiang University School of Medicine, Hangzhou 31058, China

Abstract

Glioma treatment remains a challenge owing to unsatisfactory targeted chemotherapy, where the blood–brain barrier (BBB) hinders the efficient uptake of therapeutics into the brain. Vasculogenic mimicry (VM) formed by invasive glioma cells negatively affects the treatment of glioma. Herein, we developed a targeted biomimetic drug delivery system comprising a doxorubicin-loaded platelet membrane-coated nanogel (DOX@PNGs). The nanogels provide great redox/pH dual responsiveness, while the platelet membrane (PLTM) promotes stability and circulation time. In vitro cellular uptake and in vivo imaging experiments demonstrated that the DOX@PNGs delivery system could penetrate the BBB, target gliomas, and destruct VM. DOX@PNGs increased drug penetration and prolonged mouse survival time during the treatment of orthotopic gliomas. These results indicate this biomimetic drug delivery system to be promising for glioma treatment and may be clinically translated in the future.

Keywords: Glioma, Blood–brain barrier, Biomimetic drug delivery system, Vasculogenic mimicry, Platelet membrane, Nanogel

Introduction

Glioblastoma multiforme (GBM), the most malignant tumour of the central nervous system (CNS), poses a major threat to human health owing to its late diagnosis, rapid progression, and ease of recurrence (Chai et al. 2017; Xue et al. 2017). Currently, surgical resection and postoperative chemoradiotherapy are used in the clinical setting (Kaynar et al., 2021; Li et al. 2021b; Weller et al. 2021). The blood–brain barrier (BBB) presents a major obstacle for therapeutic drugs targeting gliomas to overcome (Huang et al. 2021; Shi et al. 2019; Xue et al. 2017). Furthermore, the excessive use of glioma-treating drugs has been shown to result in systemic toxicity and drug resistance in oncological clinical practice (Min et al. 2022). In addition, vasculogenic mimicry (VM), which is induced by conditions such as hypoxia, is prevalent around solid tumours and can drive malignant tumour invasion (Cai et al., 2020; El Hallani et al. 2010; Ge et al. 2018). Driven by these circumstances, the most promising clinical strategy for improving GBM treatment is the development of vectors capable of effectively crossing the BBB and delivering drugs to block tumour angiogenesis (Weller et al. 2021).

The nanodrug delivery system (NDDS) has drawn researcher attention because of its potential to improve the bioavailability of therapeutic drugs (Zhang et al. 2022). Nanotechnology addresses the pitfalls of standard medications in specifically targeting tumour tissue, where nonspecific drug action results in considerable adverse effects (Sun et al. 2014; Zhen et al. 2019). Nanogels are widely employed as drug carriers because of their ability to wrap proteins, peptides, and hydrophilic drugs (Zhou et al. 2021). Many studies have reported a higher targeting efficacy by modifying peptides (Shemetov et al. 2012), and some researchers have produced nanogels (NGs) to effectively treat GBM models by integrin overexpression (Chen et al. 2017), as well as the rapid release of encapsulated drugs by polyethene glycolysis nanographene oxide (NGO-SS-mPEG) (Wen et al. 2012). However, nanomaterials are easily recognized by blood immune cells and activate the immune system, which presents a major challenge (Fang et al. 2018; Hatakeyama et al. 2011).

Bio-nanoparticles can deliver targeted effects that are precise and can evade the immune system through reciprocal recognition between cells (Gu et al. 2021) originating from cancer cells (Chen et al., 2017; Pereira-Silva et al. 2020), red blood cells (Fang et al. 2018; Lin et al. 2023), and platelets (Gu et al. 2021; Jiang et al. 2020; Li et al. 2021a). Jiang et al. reported that bio-nanoparticles (Fe_3O_4-SAS@PLT) could significantly boost cancer cell clearance and immunogenicity, suggesting a strong potential for inhibition of tumour metastasis (Jiang et al. 2020). Zhang et al. synthesized neutrophil membrane-encapsulated nanoparticles for the treatment of rheumatoid arthritis and showed that it greatly reduced synovial inflammation and acted as a joint protector (Zhang et al. 2018).

Platelets are derived from megakaryocytes, and following the appearance of a wound, they congregate near the injured blood vessels, producing substances that aid in the prevention of bleeding (Koupenova et al. 2019). It has been verified that CD62P expressed on the platelet membrane (PLTM) surface aids in targeting tumours, while another important component, CD47, plays a vital role in preventing nanomaterials from being removed by the innate immune system (Fang et al. 2018; Li et al. 2021a). Diana et al. verified that CD47 on PLTM could assist nanoparticles in evading immune system attack (Dehaini et al., 2017). In our previous study, we reported that platelets have a range of adjuvant effects in anti-tumour therapy, especially in tumour targeting and immune escape (Wu et al. 2021).

In this study, we developed a strategy using doxorubicin (DOX)-loaded redox/pH dual-responsive NG (DOX@PNGs) to target orthotopic glioblastoma and increase therapeutic efficacy of DOX. The functional drug delivery system was localized to glioma sites via interactions with membrane surface proteins and quickly released DOX when the tumour microenvironment was responsively stimulated. According to the in vivo tests, DOX@PNGs exhibited great targeting effects and increased survival time. This method could be applied to a variety of disorders and is a promising strategy for future clinical use.

Materials and methods

Materials

The rat C6 cell line, mouse hippocampal neuronal cell line (HT22), and human monocytic leukaemia cell line (THP-1) were purchased from CAS Cell Bank; the PRP was

obtained from the rats; and the BALB/c nude mice and rats were obtained from Shanghai SLAC Laboratory Animal Co., Ltd. Doxorubicin hydrochloride, mannitol, sucrose, tris-HCL, $MgCl_2$, KCL, paraformaldehyde, phosphate-buffered saline (PBS), 5-chloro-2-formylphenylboronic acid (2-FPBA), sodium alginate (SA), ethylene imine polymer (PEI), acetone, Matrigel basement membrane matrix, and phorbol myristate acetate (PMA) were all obtained from Sigma Aldrich. The protease inhibitor cocktail was procured from Biomake, Shanghai. The BCA protein assay, CCK8 assay, JC-1 assay, and Annexin V-FITC/PI apoptosis detection kits were supplied by Beyotime, China. Foetal bovine serum (FBS) and penicillin–streptomycin were purchased from Gibco, USA. Dulbecco's Modified Eagle Medium (DMEM) and Roswell Park Memorial Institute (RPMI 1640) were obtained from Hyclone, Shanghai. Cy5-NHS dye was obtained from Solarbio, China. The rabbit anti-GAPDH, rabbit anti-MMP-2, rabbit anti-MMP-9, anti-CD47, and anti-CD62P antibodies were obtained from Hua Bio, China.

Synthesis of DOX-loaded NGs

The NGs used in this study were synthesised as follows (Xu et al. 2021). First, 3.28 mg of 2-FPBA and 15.32 mg of PEI were dissolved in 1 mL of PBS overnight at 25 °C. Thereafter, 5.6 mL of n-hexane was added to a clean 10-mL glass sample bottle, followed by the addition of 350 µL of Brij30 and an immediate 1 min vortex. Subsequently, 20 µL of 0.5% wt SA, 100 µL of DOX (6 mg/mL), and 80 µL of 2-FPBA/PEI mixture were added sequentially and swirled for 1 min after the addition of each reagent. The sample was allowed to stand at room temperature for 1.5–2.0 h, after which 3 mL of acetone was added slowly along the wall of the bottle. Red sediment appeared at the bottom as DOX-loaded NGs, while bare NGs were white; in rapid sequence, the bottle was gently inclined, and the supernatant was carefully absorbed. Finally, the sample bottle was vacuumized for 2 h.

Extraction of PLTM from PRP

The PRP was obtained from rats, and the procedure was executed as described in a previous study (Wu et al. 2021). Briefly, the PRP was transferred into a clean EP tube and centrifuged at 100 *xg* for 10 min at 4 °C. The supernatant was carefully pipetted into a clean EP tube. After centrifugation at 800 *xg* for 20 min at 4 °C, the precipitate was retained and a cell lysate buffer (25 mM sucrose, 75 mM mannitol, 1 mM KCl, 10 mM Tris/HCl, 1 mM $MgCl_2$) containing protease inhibitors (100 ×) was added; the solution was kept on ice for 15 min to fully lyse the platelet cells. The cell lysate was repeatedly freeze-thawed in liquid nitrogen and a 37 °C water bath five times, after which it was broken by an ultrasonic probe for 5 s, which was repeated 5 times at 5 s intervals. The entire process was carried out on ice to avoid high temperatures caused by the ultrasound, which could damage the proteins on the cell membrane. The PLTM precipitate was obtained by centrifugation at 21,000 *xg* for 10 min at 4 °C and stored in a − 20 °C freezer.

Preparation and characterization of PNGs

We mixed 1 mg of NGs with 2×10^8/L of PLTM sediment, and a liposome extruder was used to extrude a 200 nm polycarbonate membrane five times; PLTM-coated NGs were

then obtained. The size and zeta potential of the NGs, PLTMs, and PNGs were analysed by dynamic light scattering (DLS; Malvern, Zetasizer Nano S90, Malvern, UK), and their morphological characteristics were examined by 200 kV TEM.

The surface protein distribution of PLTMs and PNGs was assessed using Coomassie Brilliant Blue (CBB) staining. Briefly, the prepared PLTMs and PNGs were fully fragmented using an ultrasonic disruptor; then, the protein concentrations of the two samples were determined using the BCA Protein Quantitation Kit, and the samples containing SDS–PAGE loading buffer were boiled for 5 min at 95 °C. Next, 10 μL of each sample was added to the prepared 4–12% gel wells. After electrophoresis, the proteins were stained with CBB staining solution for approximately 30 min and the gel was washed with a highly concentrated decolourising solution until the gel became transparent. Finally, photographs were taken and recorded. Similarly, the expression of PLTM and PNGs surface membrane proteins (CD62P and CD47) was determined by western blotting.

In Vitro drug release

DOX release from the drug-loaded NGs was examined using the dialysis method. First, dialysis bags (MWCO = 3 kDa) with 6 mg of DOX@NGs were placed into 50 mL centrifuge tubes containing 30 mL of different release media (GSH concentration of 1.0 and 10.0 mM; pH = 5.0, 6.0, or 7.4). The centrifuge tubes were shaken at 37 °C and 100 rpm, and the liquid in the tubes was removed at specified times (0.5, 1, 2, 4, 6, 8, 10, 12, and 24 h) and replenished with the same volume of the corresponding media. Finally, the absorbance of DOX was measured at 480 nm.

In Vitro cellular uptake and immune escape

The phagocytosis efficiency of nano-formulations in C6 cells and macrophages was assessed by confocal microscopy and flow cytometry. C6 cells at a density of 1×10^5 cells per well were seeded onto 24-well plates containing cell slides and incubated for 24 h. THP-1 cells in a culture medium containing 100 ng/PMA, which induces THP-1 monocyte differentiation into macrophages, were incubated on well plates in the same manner. The cell medium was then replaced with DOX, DOX@NGs, or DOX@PNGs at a final DOX concentration of 5 μg/mL. After incubation for 4 h, the cells were digested with trypsin into a single-cell suspension, and fluorescence was quantified by flow cytometry (FC500, Beckman Coulter, USA). The cell slide was washed twice with PBS, fixed in a 4% paraformaldehyde solution for 15 min, and washed three times with PBS. Subsequently, the cells were stained with 0.5 μg/mL DAPI for 15 min and washed three times with PBS. Finally, the slides were sealed with an anti-fluorescent bursting agent and photographed by confocal laser scanning microscopy (CLSM; Leica, Germany).

Apoptosis and JC-1 assay

Apoptosis and the JC-1 assay were measured using flow cytometry and fluorescence microscopy to further detect the inhibition efficiency of the drug on C6 cells. Briefly, C6 cells were seeded at a density of 5×10^5 cells/well in 6-well plates. After incubation for 24 h, the medium was replaced with DOX, DOX@NGs, DOX@PNGs, or DMEM for another 24 h. Immediately, the cells were collected using trypsin and centrifuged at

200 *xg* for 3 min. Subsequently, the cells were stained according to the Annexin V-FITC/PI apoptosis kit or JC-1 assay kit, and mitochondrial damage and apoptosis of C6 cells were detected by flow cytometry, respectively (FC500, Beckman Coulter, USA). The data were analysed using FlowJo 7.6 software. In addition, we captured a fluorescence graph of JC-1 using microscopy.

In Vitro BBB model assay

We used the Transwell model to simulate the BBB in vitro. b End.3 cells were spread in Transwell chambers at 1×10^5 cells per well, incubated at 37 ℃ on a shaker at 50 rpm, and protected from light; the fluorescence content of each group was then analysed by confocal microscopy and flow cytometry 24 h after incubation.

In Vitro destruction of VM

Fifty microlitres of Matrigel was pre-capped in 96-well plates and incubated for 30 min at 37 ℃. C6 cells (1×10^4 cells per well) were suspended in an FBS-free medium containing DOX, DOX@NGs, or DOX@PNGs at a DOX concentration of 5 μg/mL and seeded into a well plate. After incubation for 8–10 h, photographs were captured by microscopy. The percentage of tube formation was quantified using Image Pro Plus software version 6.0.

Western blotting

C6 cells were seeded in 6-well plates at a density of 5×10^5 cells per well and allowed to reach 60% confluence. The medium was then replaced with FBS-free DMEM containing DOX@PNGs and control formulations. After 24 h of incubation, the plate was washed three times with PBS after the liquid was removed. Cell lysate (RIPA:PMSF = 50:1) was added to the wells and the plates were placed on ice for 20 min, after which they were fully scraped using a spatula. The bicinchoninic acid (BCA) protein assay kit (Beyotime) was used for quantitative detection. A 12% SDS–PAGE gel was loaded with 20 μg of protein samples from each group; the protein was separated by electrophoresis at 80 V followed by 120 V and then transferred to a polyvinylidene difluoride (PVDF) membrane, which was blocked in 5% skim milk for 1 h. The PVDF membrane was subsequently washed with TBST (0.5% Tween-20 in Tris-buffered saline) and incubated with the primary antibody according to its recommended dilution at 4 °C overnight. The membranes were washed three times with TBST and incubated with an HRP-labelled secondary antibody for 1 h at room temperature. Finally, the membranes were imaged using Immobilon Western HRP substrate (Millipore, USA) on a Bio-Rad Chemioc MP system (Bio-Rad Laboratories, USA).

In Vivo anti-tumour efficacy

C6 glioma-bearing mice were established as previously described. At 7 days after model establishment, mice were randomly divided into four groups (saline, DOX, DOX@NGs, and DOX@PNGs) of 10 mice each; mice treated with saline were used as controls. Each of the above agents (at a dose of 2.5 mg DOX/kg) was injected every 3 days for a total of five injections. Mice were injected intraperitoneally with 200 μL of luciferase at a concentration of 15 mg/mL and anaesthetised with isoflurane 10 min after

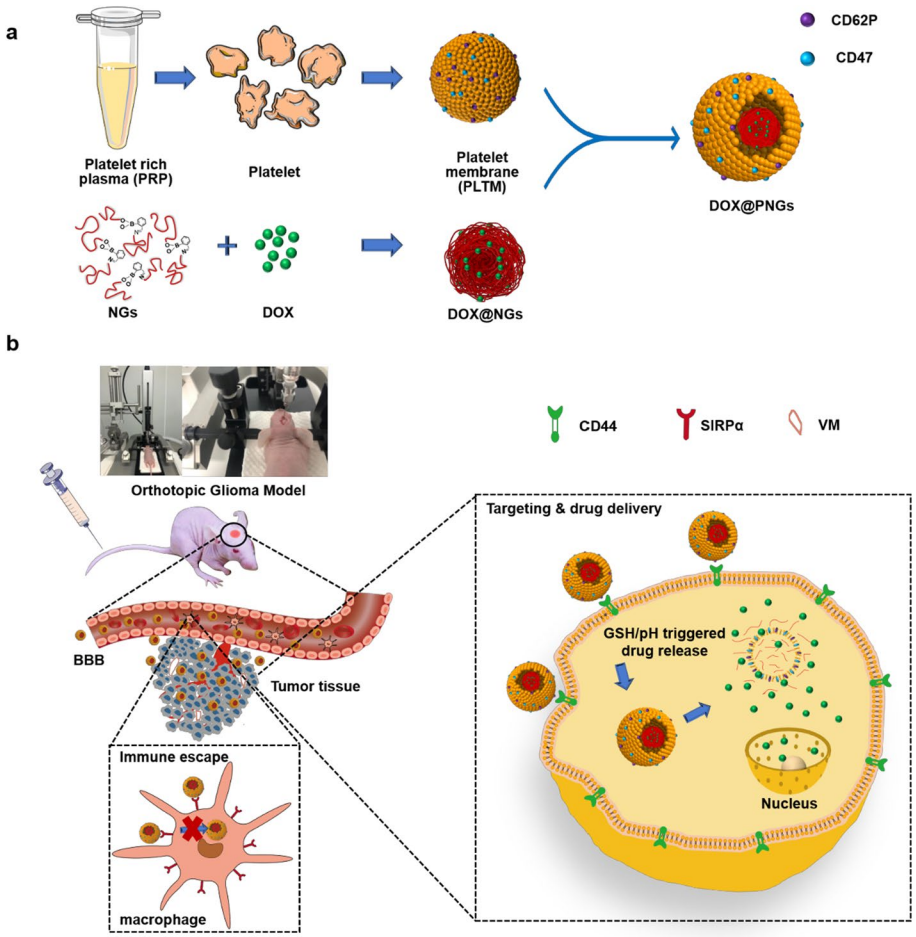

Scheme 1 **a** schematic illustration of the DOX@PNGs preparation process. **b** Treatment of brain tumours with DOX@PNGs

injection. Subsequently, tumour volume changes were observed using the NIR fluorescence imaging system IVIS III (PerkinElmer, USA) at 7, 10, 13, 16, and 19 days after modelling. Overall survival was managed, and the weight was recorded every other day. At 1 day after the last dose, three mice were randomly selected from each group, and blood was obtained from their eyes for analysis of blood biochemical parameters (ALT, AST, CREA, and urea) using a fully automated biochemical analyser (AU5800, Beckman Coulter). The brains and major organs were subjected to HE staining, IHC staining (Ki67, Caspase 3, CD34-PAS double staining), and TUNEL. The survival time of the remaining mice was observed until death.

Statistical analysis

GraphPad Prism 8 software (San Diego, CA, USA) was used for statistical analysis of the experimental results. The diversity between groups was analysed using an unpaired *t* test. The results of more than three independent repeated experiments were expressed as the mean ± SD. The overall survival was compared using the log-rank (Mantel–Cox) test. $P < 0.05$, 0.01, and 0.001 were considered statistically significant and are denoted as *, **, and ***, respectively (Scheme 1).

Results and discussion

Preparation and characterization of DOX@PNGs

Recently, bio-nanoparticles have received increasing attention due to their excellent biological activity. Among the various membrane biomaterials, PLTMs, given their multitude of interactions with other cell types, have attracted much attention due to their significant tumour targeting and immune escape potential (Wang et al. 2023; Yu et al. 2022). In this study, we aimed to leverage these unique abilities to design a pH/glutathione (GSH) dual-responsive bio-nanogel delivery system (Xu et al. 2021). The PLTM fragment was isolated from rats' platelet rich plasma (PRP) through differential centrifugation and freeze–thaw processes and then coated onto an NG core. The sizes of the NGs, PLTMs, and PLTM-coated NGs (PNGs) were 92.07 ± 0.95 nm, 174.3 ± 2.7 nm, and 119.1 ± 1.2 nm, respectively (Fig. 1A, B). The zeta potentials of the NGs, PLTMs,

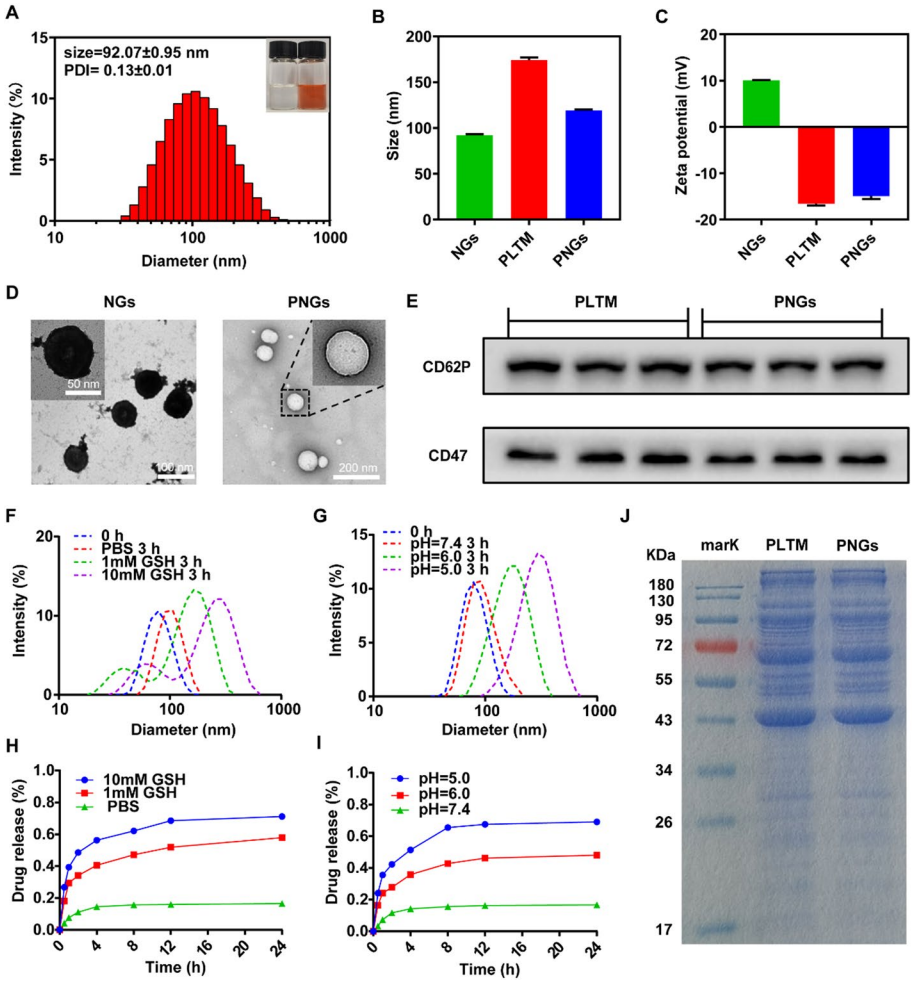

Fig. 1 Characterization of NGs, PLTM, and PNGs. **A** Size distribution of NGs determined by DLS. **B**, **C** Z-average size and surface zeta potential of the NGs, PLTM, and PNGs; $n = 3$. **D** Representative TEM images of NGs and PNGs. **E** Expression of PLTM and PNGs surface proteins CD62P and CD47, respectively. **F**, **G** Particle size variation of NGs under different GSH concentrations or different pH conditions. **H**, **I** DOX release from biomimetic nanodrugs under different concentrations of GSH or different pH conditions. **J** CBB staining patterns of the NGs and PNGs

and PNGs were 10.06 ± 0.04 mV, − 14.9 ± 0.6 mV, and − 16.5 ± 0.4 mV, respectively (Fig. 1C). The NGs of PNGs was approximately 120 nm in size, which can easily be taken up into glioma cells [30]. In the transmission electron microscopy (TEM) images, the NGs appeared spherical and regularly sized in morphometric terms (Fig. 1D), while conjugation with the PLTM increased the NG size and decreased the zeta potential.

Sodium salt-–polyacrylamide gel electrophoresis (SDS–PAGE) was performed to assess the protein expression of PNGs and PLTM. There was no significant change in protein expression between PNGs and PLTMs (Fig. 1J), suggesting the PLTM was successfully coted on the NGs. CD62P and CD47 were expressed on the membrane surface of PNGs, as determined by western blotting (Fig. 1E), indicating that PLTM surface protein was not affected throughout the production process. CD62P (P-selectin) has been reported to closely interact with tumour cell membranes (Jiang et al. 2020; Li et al. 2021a). CD47 is responsible for binding to SIRPα on the surface of macrophages, which protects nano-agents from immune system attack (Fang et al. 2018; Jiang et al. 2020). In addition, the NGs remained stable in a 10% FBS medium for 1 week at 37 °C (Additional file 1: Fig. S1). The size of the NGs did not change significantly over time. Finally, we exposed the NGs to various GSH concentrations (1 mM and 10 mM) and pH values (5.0 and 6.0). When the NGs were stimulated with high concentrations of GSH and low pH, the particle size changed significantly (Fig. 1F, G), which was superior to the previously described nano-delivery system with a single stimulus (Wu et al. 2022; Zheng et al. 2022). Moreover, the sustained-release behaviour of DOX from DOX@PNGs may prolong drug action time and enhance antitumour efficacy (Fig. 1H, I).

Evaluation of cellular uptake and immune escape

The cellular uptake of different formulations in C6 cells was used to assess the ability of nano-agents to be deposited around glioma cells and was assessed by fluorescence microscopy and flow cytometry. The confocal findings showed that DOX@NGs and DOX@PNGs had enhanced tumour cell uptake efficiency compared to the free drug DOX (Fig. 2A, C) in a time-dependent manner (Additional file 1: Fig. S3). Furthermore, DOX@PNGs showed the highest fluorescence intensity by flow cytometry (Fig. 2B). Our results demonstrated that PLTMs enhanced the targeting ability of NGs in C6 cells. Considering the enhanced immune escapability of PNGs with macrophages in vitro, we co-incubated macrophages with different drugs (DOX, DOX@NGs, and DOX@PNGs) for 4 h to detect the NGs' ability to avoid immune cell clearance. Both confocal and flow cytometry revealed that DOX@PNGs were better able to evade immune clearance (Fig. 2D–F). These findings suggest that the PLTM has a protective effect in NGs via specific surface proteins, which are homologous to blood cells (Jiang et al. 2020; Wu et al. 2021).

in vitro killing efficacy of glioma cells

We assessed the inhibitory effects of the different formulations on C6 cells using the CCK8 assay. First, the tests showed that polymers with low toxicity retained more than 90% of live cells at doses of 20–100 μg/mL for both bare NGs and PNGs (Additional file 1: Fig. S2A). We then co-incubated different preparations with C6 cells at a final concentration of 5 μg/mL DOX for 24 h. Compared with the control group, the DOX@

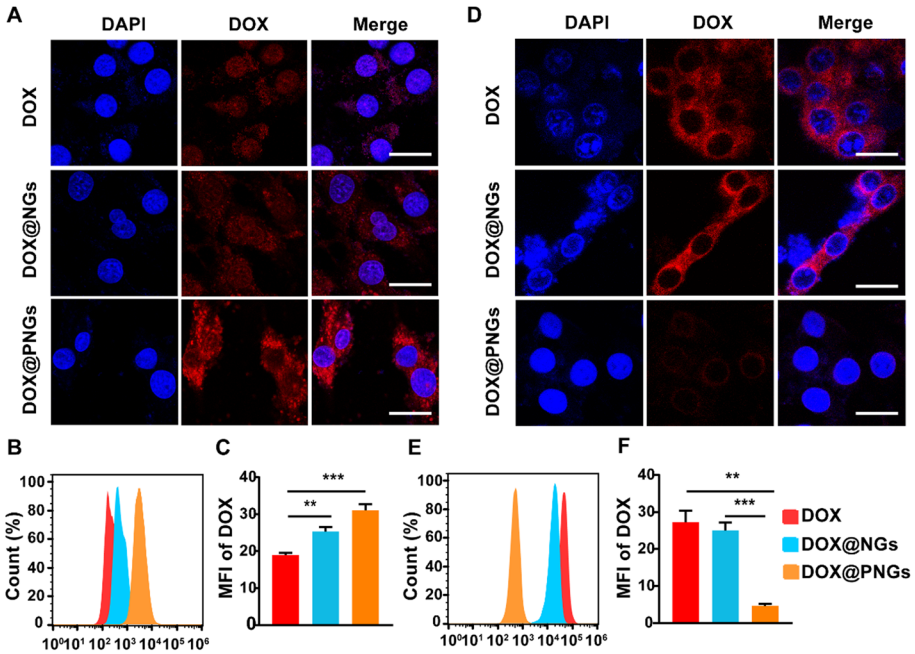

Fig. 2 in vitro cellular uptake and endosomal escape of NPs measured by CLSM and flow cytometry. **A** The confocal fluorescence images of C6 cells incubated with DOX, DOX@NGs, or DOX@PNGs with the same DOX concentration of 5 μg/mL for 2 h; red = DOX, blue = nuclei; scale bars = 25 μm. **B** Flow cytometry analysis of C6 cells incubated with DOX, DOX@NGs, or DOX@PNGs with the same DOX concentration of 5 μg/mL for 2 h. **C** Quantification of the mean fluorescence intensities of the C6 cells. Data represent the means ± SD, $^{**}p < 0.01$, $^{***}p < 0.001$. **D** The confocal fluorescence images of macrophage cells incubated with DOX, DOX@NGs, or DOX@PNGs with the same DOX concentration of 5 μg/mL for 2 h; red = DOX, blue = nuclei; scale bars = 50 μm. **E** Flow cytometry analysis of macrophage cells incubated with DOX, DOX@NGs, or DOX@PNGs with the same DOX concentration of 5 μg/mL for 2 h. **F** Quantification of the mean fluorescence intensities of the macrophage cells. Data represent the means ± SD, $^{**}p < 0.01$, $^{***}p < 0.001$

PNGs group had much lower cell viability at all doses—particularly at 20 μg/mL, where cell viability was less than 20%—indicating significantly improved antitumour activity (Additional file 1: Fig. S2B). We further demonstrated the ability of different agents to induce apoptosis using the Annexin V-FITC/PI double staining assay. The percentage of early- and late-stage apoptosis in the DOX@PNGs group was 35.03%, whereas that in the other groups was less than 10% (Fig. 3A, C). In addition, we used the JC-1 assay to assess the capacity of each treatment group to cause mitochondrial damage. Normal mitochondria emit intense red fluorescence; in contrast, unhealthy mitochondria fluoresce green due to a decrease in membrane potential (Ruan et al. 2019). C6 cells treated with DOX@PNGs showed significantly more green fluorescence signals (Fig. 3B, E). There was a significant difference in the JC-1 monomer/polymer fluorescence ratio in the DOX@PNGs group compared to the DOX and DOX@NGs groups (Fig. 3D). The above experiments show that PLTM-modified drug-loaded NGs have stronger cytotoxic effects.

in vitro and in vivo BBB penetration

The BBB greatly hinders the delivery of chemotherapeutic agents to brain tumours in situ (Xue et al. 2017). To investigate the BBB penetration ability of different nano

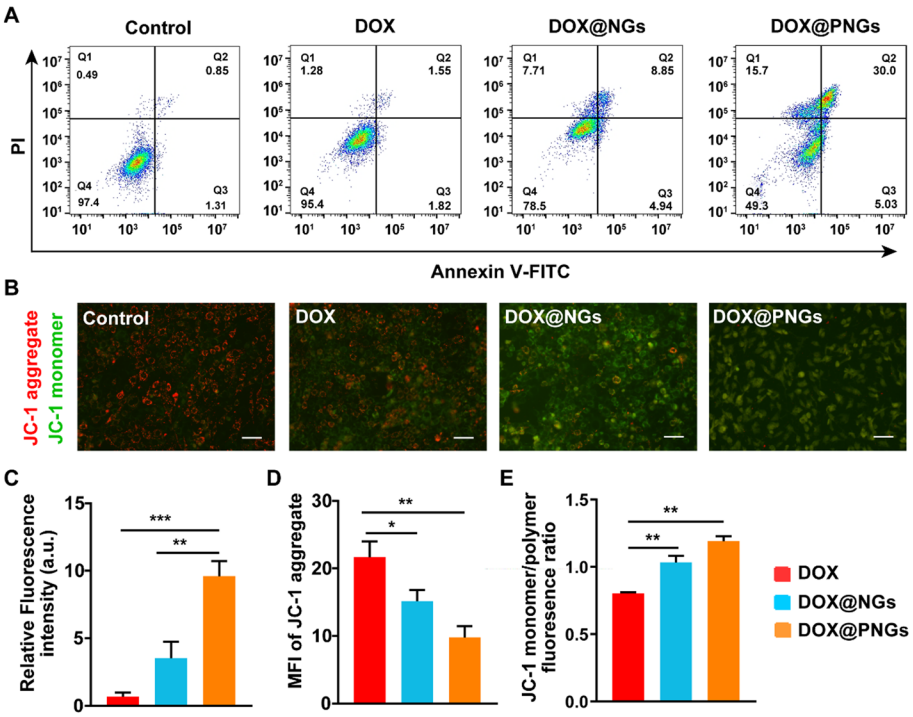

Fig. 3 in vitro tumour killing effect. After C6 cells were incubated with DOX, DOX@NGs, or DOX@PNGs at the same DOX concentration of 5 μg/mL for 24 h, **A** the Annexin V-FITC/PI detection kit was used to detect their ability to undergo apoptosis induced by various nano-preparations. **B** Fluorescence images of the mitochondria of C6 cells damaged by NGs; red = normal mitochondria; scale bar = 100 μm. **C** Flow cytometry quantitative analysis of the ability of different preparations to induce apoptosis in C6 cells; $n = 3$. **D** Quantification of the mean fluorescence intensities of the C6 cells of the JC-1 aggregate calculated according to **B**. **E** Flow cytometry analysis of the ratio of JC-1 monomer/polymer in the mitochondria of C6 cells; $n = 3$. Error bars represent the means ± SD; $n = 3$; *$p < 0.05$, **$p < 0.01$, ***$p < 0.001$

formulations, we constructed an in vitro BBB model using vascular endothelial cells. Confocal images showed red fluorescence around C6 cells in the DOX@PNGs group, while there was a low fluorescence intensity of free DOX; this further confirmed the inability of DOX to cross the BBB (Fig. 4C, E). The flow cytometry results demonstrated that the BBB permeability of DOX@PNGs was 36.4%, which was significantly higher than that of DOX (Fig. 4B). The fluorescence intensity of DOX@PNGs was also significantly stronger than the DOX and the DOX@NGs, indicating its remarkable BBB penetration ability.

Furthermore, we used Cy5-stained NGs to demonstrate the in vivo BBB penetration and targeting abilities of the PNGs using an in vivo imaging system (IVIS). By tail vein injection of different agents (Cy5, Cy5-NGs, and Cy5-PNGs), we obtained a fluorescence distribution photo at the expected time (Additional file 1: Fig. S4A). Cy5-PNGs showed a strong fluorescent signal in the brain 1 h after injection, reaching a maximum at 6 h, while partial fluorescence could still be detected after 24 h. In contrast, the fluorescence intensity of free Cy5 and Cy5-NGs reached its maximum at 3 h post-injection, and both were lower than that of Cy5-PNGs, especially Cy5. We hypothesized that CD62P on the PLTM could pass through the BBB, which allowed the fluorescence intensity of Cy5-PNGs to reach its maximum 6 h after injection and

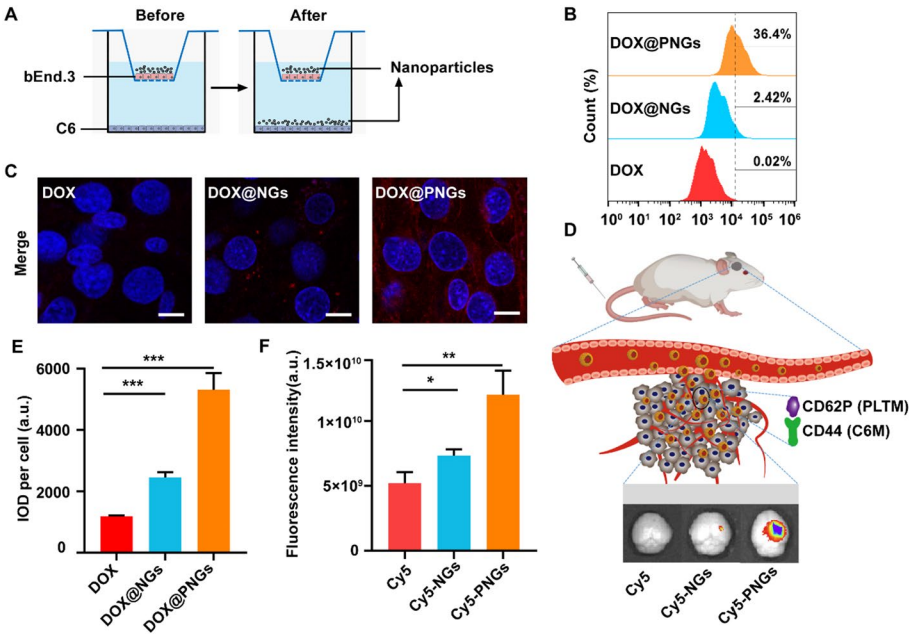

Fig. 4 Evaluation of BBB penetration efficiency by in vitro and in vivo models. **A** In vitro blood–brain barrier model. **B** Flow cytometry analysis of the fluorescence intensity of C6 cells in the in vitro BBB model. **C** Confocal microscope map of C6 cells incubated with DOX, DOX@NGs, or DOX@PNGs with same DOX concentration of 5 μg/mL for 24 h; scale bar = 20 μm. **D** IVIS image of the mouse brain 24 h after free Cy5, Cy5-NGs, or Cy5-PNGs injection via the tail vein. **E** Fluorescence semi-quantitative analysis of **C**. **F** Flow cytometry analysis of the relative fluorescence intensity of C6 cells in the in vivo BBB model. The error bars represent the means ± SD; $n = 3$; $^{*}p < 0.05$, $^{**}p < 0.01$, $^{***}p < 0.001$

then gradually decrease. The isolated organ fluorescence map showed that the fluorescence intensity of Cy5-PNGs was 2.3 times that of Cy5 and 1.64 times that of Cy5-NGs after 24 h (Fig. 4D, F), and fluorescence semi-quantitative analysis showed a significant difference between the groups (Additional file 1: Figure S4B, C). in vitro and in vivo BBB penetrating assays revealed that the constructed biomimetic NGs could target tumours effectively.

Destruction of vasculogenic mimicry (VM)

The aggressive nature of tumours is inextricably linked to the abundance of surrounding blood supply. We used a previously reported stromal gel model to assess the ability of DOX@PNGs to inhibit VM in C6 cells (Ruan et al. 2019). After 10 h, untreated C6 cells quickly formed vascular-like channels at the bottom of the well plates. In contrast, the cells treated with DOX@PNGs had only a small fraction of vascular-like channels, and sometimes none (Fig. 5B, D). This indicates that DOX@PNGs can effectively inhibit VM in glioma cells. To investigate the molecular mechanism of VM destruction, the expression levels of VM-related indicators, such as matrix metalloproteinase-2 (MMP-2) and matrix metalloproteinase-9 (MMP-9), were determined by western blotting (Fig. 5C). After treatment with different formulations for 24 h, the expression levels of MMP-2 and MMP-9 were downregulated in C6 cells compared to those in untreated cells. In particular, C6 cells treated with DOX@PNGs showed the lowest indicator protein expression, indicating that DOX@PNGs could efficiently downregulate indicator protein expression

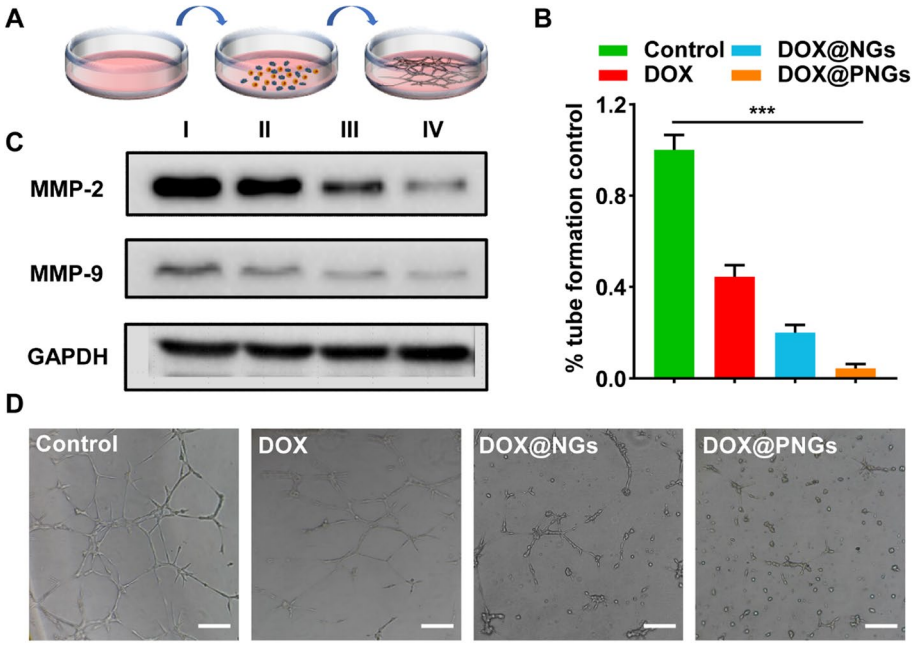

Fig. 5 in vitro matrix gel model inhibition and anti-vasculogenic mimicry evaluation. **A** Schematic diagram of VM model. **B** The proportion of tubular channels in the control group. Error bars represent the means ± SD; $n = 3$; ***$p < 0.001$. **C** Protein expression levels of MMP-2 and MMP-9 in C6 cells; I, II, III, and IV = control, DOX, DOX@NGs, and DOX@PNGs, respectively. **D** Vasculogenic mimicry of C6 cells in vitro after co-culture with control, DOX, DOX@NGs, or DOX@PNGs for 10 h; scale bar = 20 μm

in C6 cells. However, the VM-destruction effect of DOX is probably due to its cytotoxicity. These evidences indicate that our prepared biomimetic delivery system could effectively inhibit the formation of glioma vasculogenic mimicry, which is significant for enhancing chemotherapeutic effects.

in vivo antitumour efficacy

The in vivo antitumour efficacy of biomimetic NGs was evaluated in an orthotopic glioma-bearing mouse model. Haematoxylin and eosin (HE) staining (Fig. 6E) of the brain showed that the tumour cells in the saline group were close, numerous, and tightly arranged, with darkly stained nuclei. In addition, the tumour tissue treated with free DOX and DOX@NGs was loosely arranged, while the DOX@PNGs group had the most sparsely arranged tumour cells, indicating that the DOX@PNGs possessed the highest inhibitory effect. We also performed immunohistochemical (IHC) staining (Fig. 6E) of brain tissue to investigate the expression of proliferation (Ki67) and apoptosis (caspase 3 and CC3) markers in different groups of glioma-bearing mice. The DOX@PNGs group exhibited the highest apoptosis

(See figure on next page.)

Fig. 6 in vivo tumour suppression in orthotopic glioma model mice. **A** An orthotopic glioma model was established with the C6 cell line in 4 to 6-week-old nude male mice. Control, DOX, DOX@NGs, and DOX@PNGs were intravenously injected 7 day post-tumour implantation at the indicated days. The tumour tissues were collected for analysing the blood gain and organs (HE and IHC staining) 1 day after the final injection. **B** IVIS images of glioma growth in mice on the 7th, 10th, 13th, 16th, and 19th day after injection with as-fabricated NPs; red = strong fluorescence signal. **C** Schematic map of mice brain anatomical specimen. **D** Survival curve of mice in each group; $n = 7$; *$p < 0.05$, ***$p < 0.001$. **E** HE staining, IHC staining, and CD34-PAS double staining of mouse brain tissue after different treatments. Scale bar = 50 μm

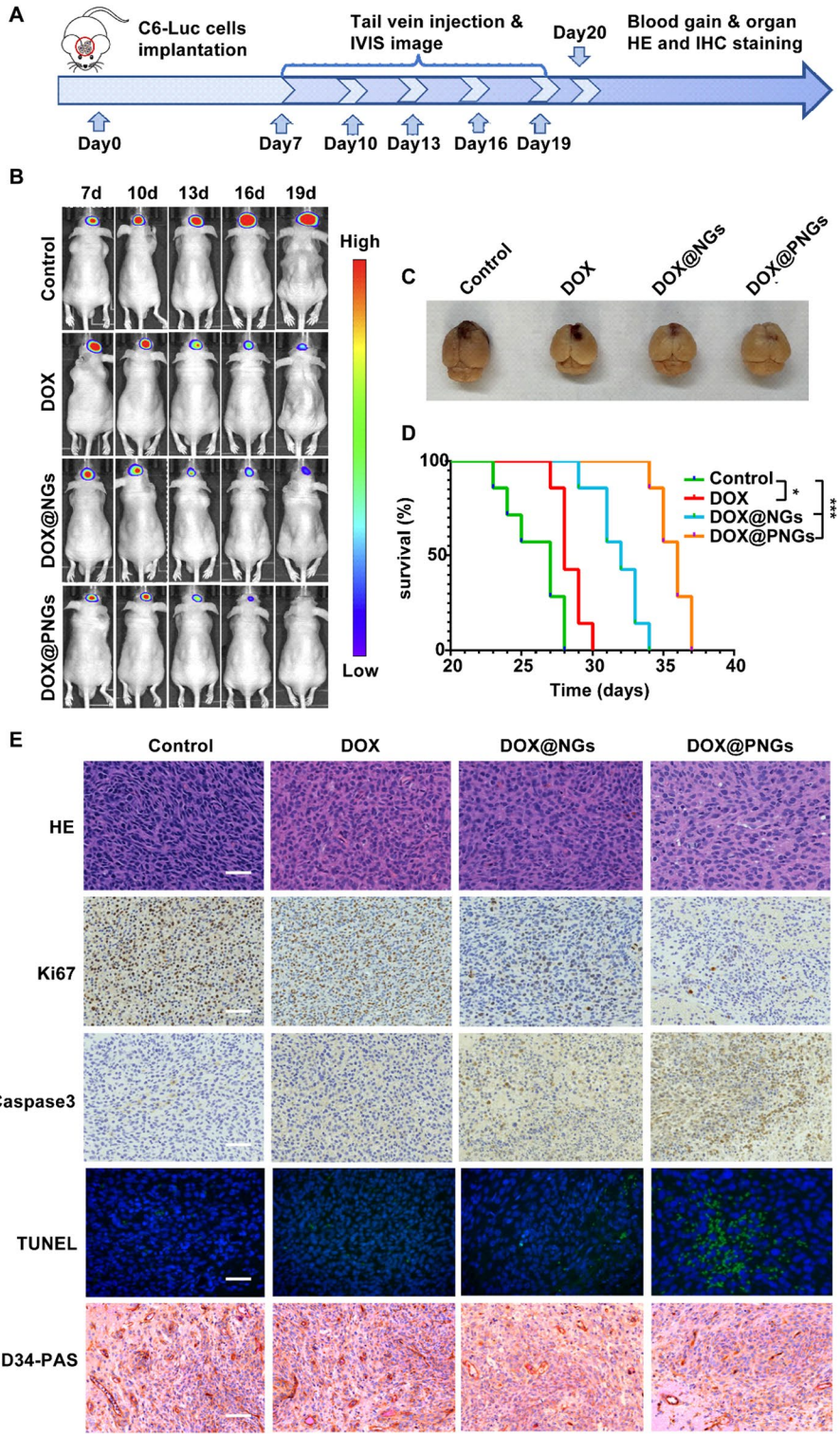

Fig. 6 (See legend on previous page.)

rate compared with the saline, free DOX, and DOX@NGs groups. In addition, Ki67 expression in mice treated with DOX-PNGs was remarkably decreased. A glioma model was constructed using Luc-C6 cells to image brain tumours using chemiluminescence (Fig. 6B).

Mice treated with DOX@PNGs had the smallest tumour volumes, revealing its valuable antitumour effect. These results confirm the superiority and therapeutic efficacy of the targeted modified biomimetic NGs. Finally, we performed transferase-mediated dUTP-biotin nick end labelling (TUNEL) to assess tumour tissue apoptosis, which showed that the green fluorescence intensity was stronger in the DOX@PNG group than in the other formulations (Fig. 6E), indicating significant apoptosis of glioma cells in mice treated with DOX@PNGs. PAS-CD34 double staining illustrated the vigorous VM inhibition effect of the DOX@PNGs group, which was consistent with the results of previous experiments. Kaplan–Meier survival curves showed that DOX@PNGs significantly prolonged the lifespan of mice (Fig. 6D). The median survival time (MST) was significantly longer in the DOX@PNGs group (34.5 days) than in the saline (23 days), DOX (27 days), and DOX@NGs (31 days) groups. These results suggested that DOX@PNGs had the best anti-glioma activity, with significant tumour growth inhibition in all groups (Fig. 6C); this may be attributed to BBB penetration resulting in drug aggregation at the tumour site. DOX@NGs also showed slightly better tumour suppression than free DOX but were much less effective than DOX@PNGs, suggesting a weak antitumour effect due to poor targeting ability. On the other hand, the poor performance of free DOX was presumably due to its inability to penetrate the BBB. Overall, the anti-tumour activity of DOX@PNGs was found to be outstanding through both in vitro and in vivo assessments.

in vivo safety

The biosafety of the nano-formulations was assessed by histopathology and blood analysis. HE staining (Fig. 7A) showed no significant difference between tissues from mice treated with DOX@PNGs and normal mice. In contrast, mice treated with DOX exhibited myocardial fibrous disruption, alveolar wall thickening, and inflammatory cell infiltration, which is consistent with the side effects of DOX. In addition, the haematological parameters of mice treated with DOX@PNGs were relatively stable compared with those of the other treatment groups. Blood levels of aspartate aminotransferase (AST), alanine aminotransferase (ALT), creatinine (CR), and uric acid (UA) showed that DOX caused mild liver and nephrotoxicity (Fig. 7B–E). However, encapsulation with PLTMs ameliorated the hepatic and renal toxicity induced by DOX, owing to the ability of DOX@PNGs to target glioma sites, release the drug rapidly, and reduce the nonspecific aggregation of the drug in the organs in vivo. We also found that DOX@NGs exhibited slightly higher hepatorenal toxicity than DOX@PNGs, which we speculate is due to the lack of PLTM modification, resulting in the inability to specifically target the tumour site with the drug, leading to relatively more drug distribution to the liver and kidney tissues. Thus, these results confirm that DOX@PNGs have relatively little effect on liver and kidney function in mice. Our study confirmed that DOX@PNGs have good biocompatibility in living organisms, do not cause side effects in normal tissues, and can be safely applied in biological experiments.

Conclusions

In summary, we developed a biomimetic NG by leveraging PLTMs, which has strong anti-glioma effects and could effectively cross the BBB and destruct VM in glioma therapy. The enhanced tumour reaction of DOX@PNGs is mainly mediated by CD62P–CD44 on the surface of PLTMs both in vitro and in vivo. This research

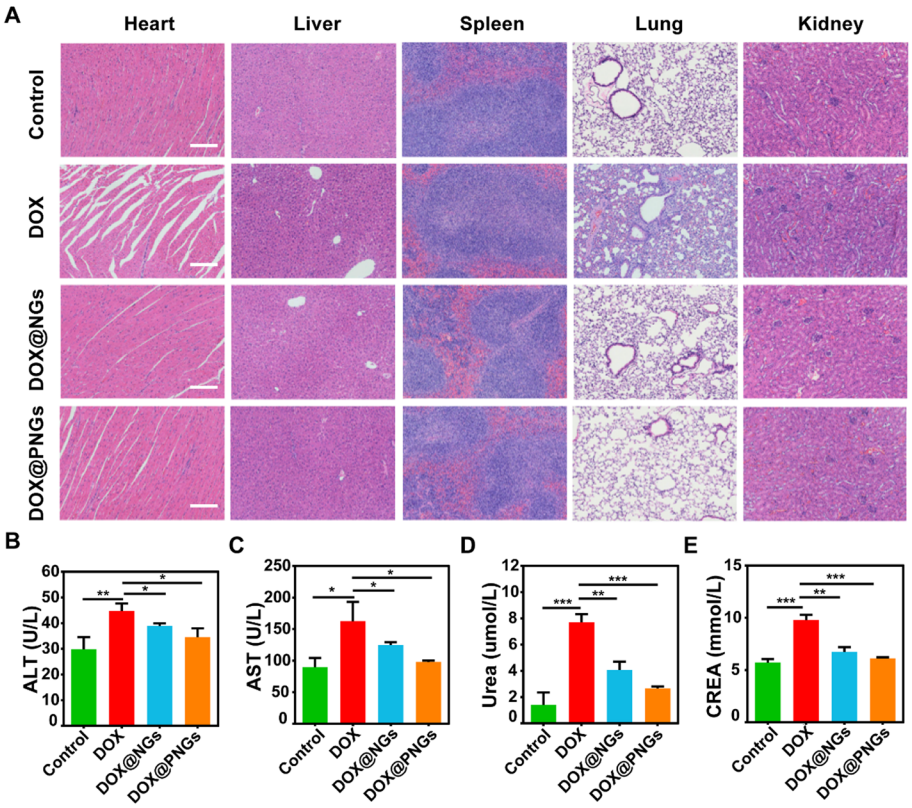

Fig. 7 Biological safety of NPs in vivo. **A** Images of organ tissue sections after treatment with different nanocarriers and drugs. Sections were subjected to HE staining; scale bar = 200 μm. **B**–**E** Test results for liver and renal function. The error bars represent the means ± SD; $n = 3$; *$p < 0.05$, **$p < 0.01$, ***$p < 0.001$

presents a potential biomimetic drug delivery system for VM-based anti-tumour drugs for glioma treatment.

Supplementary Information

The online version contains supplementary material available at https://doi.org/10.1186/s12645-023-00167-w.

Additional file 1: Figure S1. Stability of NGs and PNGs in 10% FBS for 7 days. **Figure S2.** Cell viability was measured by the CCK8 assay. **Figure S3.** Flow cytometry quantitative analysis of the ability of different preparations to induce apoptosis in C6 cells at the indicated timepoints (2, 4, and 24 h). **Figure S4.** Distribution of NPs *in vivo*.

Acknowledgements
We are deeply grateful to Professor Junjie Deng for his assistance in the preparation of doxorubicin-loaded platelet membrane-coated nanogel.

Author contributions
QL: conceptualization, investigation, formal analysis, methodology, writing original draft. JS: investigation, methodology, writing original draft. LW: investigation, formal analysis, methodology. SL: investigation. YY: investigation. WX: investigation. KH: investigation. YZ: investigation. FK: investigation. WY: investigation. YW: investigation. LP: investigation. KL: conceptualization, funding acquisition, investigation, methodology, supervision, writing—original draft, writing—review and editing. ZW: conceptualization, funding acquisition, investigation, methodology, supervision, writing—original draft, writing—review and editing. All authors read and approved the final manuscript.

Funding
This work was supported by the National Natural Science Foundation of China (8217082371); The Zhejiang Medical and Health Science and Technology Project (2022KY529); Key projects jointly constructed by the Ministry and the province of Zhejiang Medical and Health Science and Technology Project (WKJ-ZJ-2019). The Traditional Chinese Medicine Scientific Research Project of Zhejiang Province (2023ZL010).

Availability of data and materials
All data generated or analyzed during this study are included in this published article and its supplementary information file.

Declarations

Ethics approval and consent to participate
All experimental procedures and protocols were reviewed and ethically approved by the Animal Care and Use Committee of Zhejiang Provincial People's Hospital and were in accordance with the Guide for the Use and Care of Laboratory Animals.

Consent for publication
All authors have given approval to the final version of the manuscript.

Competing interests
The authors declare that they have no competing interests.

Received: 23 November 2022 Accepted: 15 February 2023
Published online: 24 February 2023

References

Cai H, Liu W, Liu X, Li Z, Feng T, Xue Y et al (2020) Advances and Prospects of Vasculogenic Mimicry in Glioma: A Potential New Therapeutic Target? OTT 13:4473–4483
Chai Z, Hu X, Wei X, Zhan C, Lu L, Jiang K et al (2017) A facile approach to functionalizing cell membrane-coated nanoparticles with neurotoxin-derived peptide for brain-targeted drug delivery. J Control Release 264:102–111
Chen W, Zou Y, Zhong Z, Haag R (2017) Cyclo(RGD)-decorated reduction-responsive nanogels mediate targeted chemotherapy of integrin overexpressing human glioblastoma in vivo. Small. https://doi.org/10.1002/smll.201601997
Dehaini D, Wei X, Fang RH, Masson S, Angsantikul P, Luk BT et al (2017) Erythrocyte-platelet hybrid membrane coating for enhanced nanoparticle functionalization. Adv Mater. https://doi.org/10.1002/adma.201606209
El Hallani S, Boisselier B, Peglion F, Rousseau A, Colin C, Idbaih A et al (2010) A new alternative mechanism in glioblastoma vascularization: tubular vasculogenic mimicry. Brain 133:973–982
Fang RH, Kroll AV, Gao W, Zhang L (2018) Cell membrane coating nanotechnology. Adv Mater 30:e1706759
Ge H, Luo H (2018) Overview of advances in vasculogenic mimicry—a potential target for tumor therapy. Research 10:2429–2437
Gu X, Gao Y, Wang P, Wang L, Peng H, He Y et al (2021) Nano-delivery systems focused on tumor microenvironment regulation and biomimetic strategies for treatment of breast cancer metastasis. J Control Release 333:374–390
Hatakeyama H, Akita H, Harashima H (2011) A multifunctional envelope type nano device (MEND) for gene delivery to tumours based on the EPR effect: a strategy for overcoming the PEG dilemma. Adv Drug Deliv Rev 63:152–160
Huang CW, Chuang CP, Chen YJ, Wang HY, Lin JJ, Huang CY et al (2021) Integrin alpha2beta1-targeting ferritin nanocarrier traverses the blood-brain barrier for effective glioma chemotherapy. J Nanobiotechnology 19:180
Jiang Q, Wang K, Zhang X, Ouyang B, Liu H, Pang Z et al (2020) Platelet membrane-camouflaged magnetic nanoparticles for ferroptosis-enhanced cancer immunotherapy. Small 16:e2001704
Kaynar A, Altay O, Li X, Zhang C, Turkez H, Uhlén M et al (2021) Systems biology approaches to decipher the underlying molecular mechanisms of glioblastoma multiforme. IJMS. https://doi.org/10.3390/ijms222413213
Koupenova M, Corkrey HA, Vitseva O, Manni G, Pang CJ, Clancy L et al (2019) The role of platelets in mediating a response to human influenza infection. Nat Commun 10:1780
Li B, Chu T, Wei J, Zhang Y, Qi F, Lu Z et al (2021a) Platelet-membrane-coated nanoparticles enable vascular disrupting agent combining anti-angiogenic drug for improved tumor vessel impairment. Nano Lett 21:2588–2595
Li Y, Ma Y, Wu Z, Xie R, Zeng F, Cai H et al (2021b) Advanced imaging techniques for differentiating pseudoprogression and tumor recurrence after immunotherapy for glioblastoma. Front Immunol 12:790674
Lin M, Li Y, Long H, Lin Y, Zhang Z, Zhan F, Li M, Wu C, Liu Z (2023) Cell membrane-camouflaged DOX-loaded β-glucan nanoparticles for highly efficient cancer immunochemotherapy. Int J Biol Macromol 225:873–885
Min X, Dingchao X, Xun Z, Cunzu W (2022) Preliminary study on relationship between Temozolomide chemotherapy-resistant cells and stem cells in gliomas. Turk Neurosurg 32:357–363
Pereira-Silva M, Santos AC, Conde J, Hoskins C, Concheiro A, Alvarez-Lorenzo C et al (2020) Biomimetic cancer cell membrane-coated nanosystems as next-generation cancer therapies. Expert Opin Drug Deliv 17:1515–1518
Ruan S, Xie R, Qin L, Yu M, Xiao W, Hu C et al (2019) Aggregable nanoparticles-enabled chemotherapy and autophagy inhibition combined with Anti-PD-L1 antibody for improved glioma treatment. Nano Lett 19:8318–8332
Shemetov AA, Nabiev I, Sukhanova A (2012) Molecular interaction of proteins and peptides with nanoparticles. ACS Nano 6:4585–4602
Shi D, Mi G, Shen Y, Webster TJ (2019) Glioma-targeted dual functionalized thermosensitive Ferri-liposomes for drug delivery through an in vitro blood-brain barrier. Nanoscale 11:15057–15071
Sun T, Zhang YS, Pang B, Hyun DC, Yang M, Xia Y (2014) Engineered nanoparticles for drug delivery in cancer therapy. Angew Chem Int Ed Engl 53:12320–12364
Wang H, Wu C, Tong X, Chen S (2023) A biomimetic metal-organic framework nanosystem modulates immunosuppressive tumor microenvironment metabolism to amplify immunotherapy. J Control Release 353:727–737
Weller M, van den Bent M, Preusser M, Le Rhun E, Tonn JC, Minniti G et al (2021) EANO guidelines on the diagnosis and treatment of diffuse gliomas of adulthood. Nat Rev Clin Oncol 18:170–186

Wen H, Dong C, Dong H, Shen A, Xia W, Cai X et al (2012) Engineered redox-responsive PEG detachment mechanism in PEGylated nano-graphene oxide for intracellular drug delivery. Small 8:760–769
Wu L, Li Q, Deng J, Shen J, Xu W, Yang W et al (2021) Platelet-tumor cell hybrid membrane-camouflaged nanoparticles for enhancing therapy efficacy in glioma. Int J Nanomed 16:8433–8446
Wu T, Liu Y, Cao Y, Liu Z (2022) Engineering macrophage exosome disguised biodegradable nanoplatform for enhanced sonodynamic therapy of glioblastoma. Adv Mater 34:e2110364
Xu W, Wang J, Li Q, Wu C, Wu L, Li K et al (2021) Cancer cell membrane-coated nanogels as a redox/pH dual-responsive drug carrier for tumor-targeted therapy. J Mater Chem B 9:8031–8037
Xue J, Zhao Z, Zhang L, Xue L, Shen S, Wen Y et al (2017) Neutrophil-mediated anticancer drug delivery for suppression of postoperative malignant glioma recurrence. Nat Nanotechnol 12:692–700
Yu Y, Cheng Q, Ji X, Chen H, Zeng W, Zeng X, Zhao Y, Mei L (2022) Engineered drug-loaded cellular membrane nanovesicles for efficient treatment of postsurgical cancer recurrence and metastasis. Sci Adv 8(49):eadd3599
Zhang Q, Dehaini D, Zhang Y, Zhou J, Chen X, Zhang L et al (2018) Neutrophil membrane-coated nanoparticles inhibit synovial inflammation and alleviate joint damage in inflammatory arthritis. Nat Nanotechnol 13:1182–1190
Zhang M, Xu N, Xu W, Ling G, Zhang P (2022) Potential therapies and diagnosis based on Golgi-targeted nano drug delivery systems. Pharmacol Res 175:105861
Zhen X, Cheng P, Pu K (2019) Recent advances in cell membrane-camouflaged nanoparticles for cancer phototherapy. Small 15:e1804105
Zheng T, Wang W, Mohammadniaei M, Ashley J, Zhang M, Zhou N et al (2022) Anti-MicroRNA-21 oligonucleotide loaded spermine-modified acetalated dextran nanoparticles for b1 receptor-targeted gene therapy and antiangiogenesis therapy. Adv Sci (weinh) 9:e2103812
Zhou X, Smith QR, Liu X (2021) Brain penetrating peptides and peptide-drug conjugates to overcome the blood-brain barrier and target CNS diseases. Wiley Interdiscip Rev Nanomed Nanobiotechnol 13:e1695

Publisher's Note